

APPLICATION OF AN IMPROVED NELSON-NGUYEN ANALYSIS TO ECCENTRIC,
ARBITRARY PROFILE LIQUID ANNULAR SEALS

Satyasrinivas Padavala and Alan B. Palazzolo
Texas A&M University
College Station, Texas

and

Pat Vallely and Steve Ryan
NASA George C. Marshall Space Flight Center
Marshall Space Flight Center, Alabama

56-37

12850

p. 23

Abstract

This paper presents an improved dynamic analysis for liquid annular seals with arbitrary profile based on a method, first proposed by Nelson and Nguyen. An improved first order solution that incorporates a continuous interpolation of perturbed quantities in the circumferential direction, is presented. The original method uses an approximation scheme for circumferential gradients, based on Fast Fourier Transforms (FFT). A simpler scheme based on cubic splines is found to be computationally more efficient with better convergence at higher eccentricities. A new approach of computing dynamic coefficients based on external specified load is introduced. This improved analysis is extended to account for arbitrarily varying seal profile in both axial and circumferential directions. An example case of an elliptical seal with varying degrees of axial curvature is analyzed. A case study based on actual operating clearances (6 axial planes with 68 clearances/plane) of an interstage seal of the Space Shuttle Main Engine High Press Oxygen Turbopump (SSME-ATD-HPOTP) is presented.

NOMENCLATURE

a_i, b_i	spatially dependent parts of first order solution
A_u, A_v, A_h	coefficients of the variables of first order axial momentum equation
B_u, B_v, B_h	coefficients of the variables of first order circumferential momentum equation
c_0	nominal clearance (m)
c_i, c_e	inlet and exit clearances (m)
c_x, c_y	x, y axis clearances of elliptical seal (m)
C_{xx}, C_{yy}	direct damping coefficients (N-s/m)
c_{xy}, c_{yx}	cross coupled damping coefficients (N-s/m)
$c(z, \beta)$	clearance function
E_x, E_y	eccentricities along x and y axes (m)
f_{r0}, f_{s0}	friction coefficients (Moody's or Hirs')
F_x, F_y	x and y components of seal force (N)
f_x, f_y	unbalance forces (N)
h_0, u_0, v_0, p_0	variables of zeroth order (steady state) equations
h_1, u_1, v_1, p_1	variables of first order (perturbed) equations
h	film thickness (m)
K_{xx}, K_{yy}	direct stiffness coefficients (N/m)
k_{xy}, k_{yx}	cross coupled stiffness coefficients (N/m)
L	length of the seal (m)
M_{xx}, M_{yy}	direct mass coefficients (kg)
m_{xy}, m_{yx}	cross coupled mass coefficients (kg)
p_{0i}	entrance pressure (Pa)
p_{0e}	exit pressure (Pa)
psr	pre-swirl ratio
R	radius of the rotor (m)
t	time (s)
u, v	axial and tangential velocities (m/s)
w	rotor surface velocity, ωR (m/s)
W	preload
X_0, Y_0	axes of the elliptical whirl orbit
z, β	axial and circumferential coordinates
ρ	density (kg/m^3)
μ	dynamic viscosity (Pa-s)
δ	ellipticity, $(c_x - c_y)/c_x$
$\epsilon, \epsilon_x, \epsilon_y$	eccentricity ratios
ψ	external load angle (rad)
ξ	entrance loss coefficient
ω	angular frequency (rad/s)

INTRODUCTION

Distortions in the interstage seals of the Space Shuttle Main Engine (SSME) High Pressure Oxygen Turbopump (ATD-HPOTP) due to mechanical and thermal loads have been investigated utilizing finite element models of the entire pump. Annular seals, initially designed with either straight or tapered clearance profile have been found to be severely distorted during the course of their operation.

Starting with Black's (1969) analysis of high-pressure seals, followed by Allaire's (1972) eccentric seal analysis and Childs' (1983) Hirs' bulk-flow model for tapered seals there has been a steady improvement in the modeling of annular seals and the agreement of their predicted behavior with experimental results.

The effect of seal distortion on the rotordynamic coefficients was first considered by Sharrer and Nunez (1989). They adapted the analysis of a plain seal to the case of a seal with wavy profile. The distorted seal profile was fitted with a clearance function in the form of a polynomial. Their analysis confirmed a marked change in rotordynamic coefficients due to a change in the seal profile. Similar results for this case were reported by San Andres (1991) using a variable properties model. Scharrer and Nelson (1990), treated a similar problem using a partially tapered seal model.

All the work reported in the literature is limited to distortion along the length of the seal. Detailed thermoelastic studies have revealed seal distortion is not limited to axial direction and a similar distortion occurs along the circumference also. An example of a distorted seal profile is shown in Fig 1. The clearances for this profile were obtained from a thermoelastic analysis.

This paper presents an improved dynamic analysis for an annular seal with arbitrary profile. The arbitrary seal profile may be due to distortion as above, or by design. The analysis used for this purpose is based on an approach, first proposed by Nelson and Nguyen. (1989). The original analysis showed good agreement with experimental results. This analysis is modified by including a more exact first order solution that accounts for the variation of perturbed variables along the circumference with a continuous interpolation.

Typically, seal coefficients are computed in a minimum film thickness coordinate system as a function of eccentricity and then transformed into the user defined coordinate system for actual application. Such a procedure is not valid for an arbitrary profile seal and a method for computing these coefficients directly in a global coordinate system is presented. In addition, a new procedure for computing seal coefficients based on external load specification is also discussed.

An example film thickness analysis for an elliptical seal with varying axial curvature, is discussed. The above improved analysis is employed to analyze a distorted interstage seal of a SSME Turbopump and the results are compared to those of a similar seal with average inlet and exit clearances.

THEORY

Bulk Flow Governing Equations

Mass conservation and force equilibrium considerations in the axial and circumferential directions for the control volumes in figures 2a and 2b yield the following bulk flow continuity, axial momentum and circumferential momentum equations for an incompressible fluid.

$$\frac{1}{R} \frac{\partial(hv)}{\partial\beta} + \frac{\partial(hu)}{\partial z} + \frac{\partial h}{\partial t} = 0 \quad (1)$$

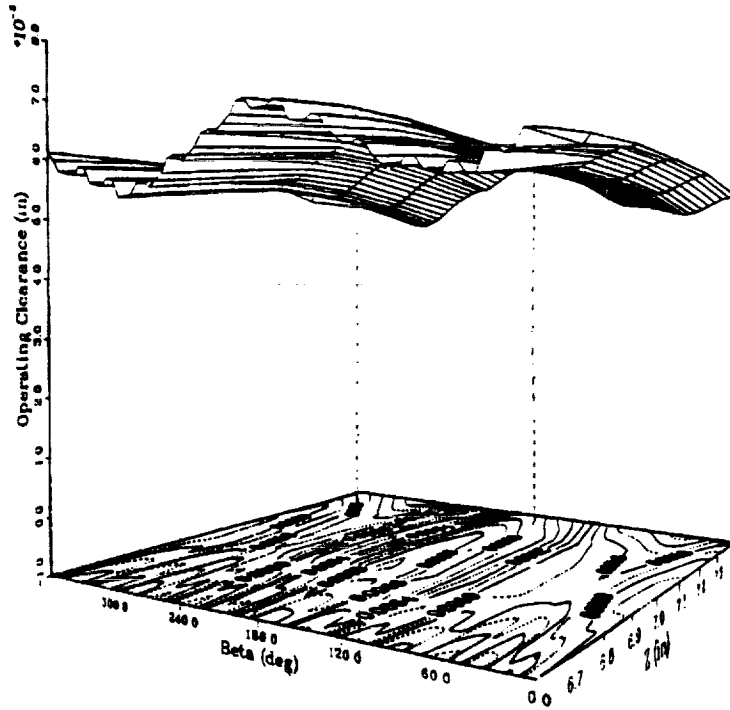


Figure 1: Predicted Clearance Profile for Turbopump Annular Seal

$$-\frac{h}{\rho} \frac{\partial p}{\partial z} = h \left\{ \frac{\partial u}{\partial t} + \frac{v}{R} \frac{\partial u}{\partial \beta} + u \frac{\partial u}{\partial z} \right\} + \bar{f}_s \frac{u}{2} \sqrt{u^2 + v^2} + \bar{f}_r \frac{u}{2} \sqrt{u^2 + (v-w)^2} \quad (2)$$

$$-\frac{h}{\rho R} \frac{\partial p}{\partial \beta} = h \left\{ \frac{\partial v}{\partial t} + \frac{v}{R} \frac{\partial v}{\partial \beta} + u \frac{\partial v}{\partial z} \right\} + \bar{f}_s \frac{v}{2} \sqrt{u^2 + v^2} + \bar{f}_r \frac{(v-w)}{2} \sqrt{u^2 + (v-w)^2} \quad (3)$$

where the friction factors \bar{f}_s and \bar{f}_r are defined for the Hirs and Moody friction factor models in the appendix.

The boundary conditions at the inlet and exit of the seal are given as,

$$p_{0i} - p_0(0, \beta) = (1 + \xi) \frac{1}{2} \rho u_0^2(0, \beta) \quad (4)$$

$$v_0(0, \beta) = psr \times \omega R \quad (5)$$

$$p_0(L, \beta) = p_{0e} \quad (6)$$

where p_{0i} and p_{0e} are the entrance and exit pressures respectively, ξ is the entrance loss coefficient and psr is the pre-swirl ratio.

Film Thickness

The expression for film thickness $h(z, \beta)$ as a function of eccentricity is derived in a fixed coordinate system, instead of a "minimum film thickness" coordinate system. The

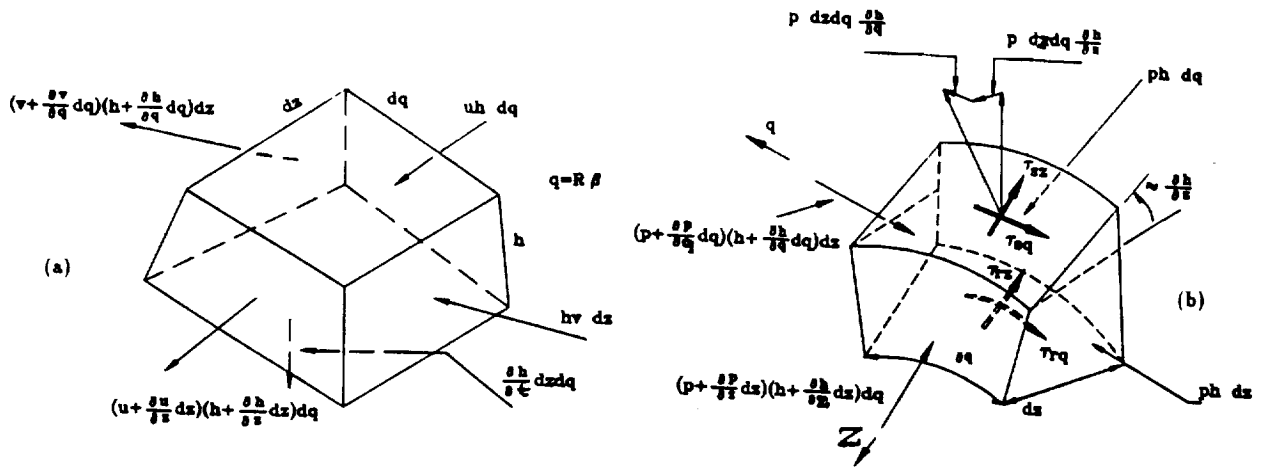


Figure 2: Differential Fluid Volumes, a) Continuity b) Momentum

coordinate system (x, y) shown in Fig. 3, is fixed at the static eccentric position and is oriented parallel to a user defined-global coordinate system. Typically, for eccentric operation of a uniform profile seal such as a straight or tapered seal, the rotordynamic coefficients are computed as a function of eccentricity in a coordinate system aligned with the line of minimum film thickness. The use of these coefficients in an application such as a stability analysis requires their transformation into the user defined coordinate system. This procedure, which is valid for a seal with uniform profile is not applicable for seals with non-uniform profile in the circumferential direction. Such seals require the computation of these coefficients in the user defined coordinate system directly, as these coefficients vary with the angle of minimum film thickness (angle of eccentricity).

The seal geometry is, in general, defined by its clearance function $c(z, \beta)$. A constant c specifies a straight seal, a linear function in z defines a tapered seal and so on. The seal profile will be non-uniform if c varies with β . The film thickness, which varies with eccentricity, is derived as a function of $c(z, \beta)$ and the eccentricity E . The expression for the film thickness and its gradients are given below with reference to Fig. 3. Besides specifying the film thickness in a fixed coordinate system, this general expression is more accurate, particularly at high eccentricities, than the more commonly used approximate form, $h_0 = c - E_x \cos \beta - E_y \sin \beta$.

$$h_0(z, \beta) = \sqrt{(R + c)^2 - (E_x \sin \beta - E_y \cos \beta)^2} - (E_x \cos \beta + E_y \sin \beta) - R \quad (7)$$

$$\frac{\partial h_0}{\partial \beta} = \frac{(R + c) \frac{\partial c}{\partial \beta} - (E_x \sin \beta - E_y \cos \beta)(E_x \cos \beta + E_y \sin \beta)}{\sqrt{(R + c)^2 - (E_x \sin \beta - E_y \cos \beta)^2}} + (E_x \sin \beta - E_y \cos \beta) \quad (8)$$

$$\frac{\partial h_0}{\partial z} = \frac{(R + c) \frac{\partial c}{\partial z}}{\sqrt{(R + c)^2 - (E_x \sin \beta - E_y \cos \beta)^2}} \quad (9)$$

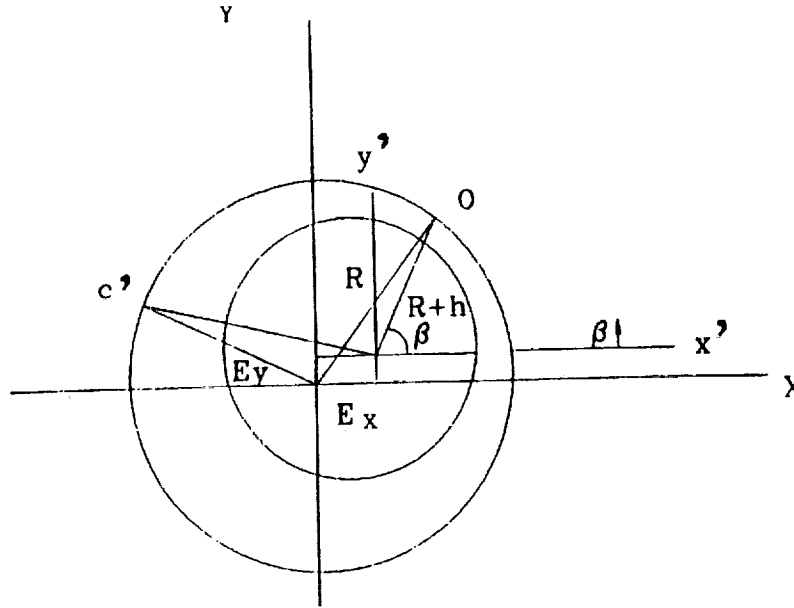


Figure 3: Diagram for Deriving General Clearance Expression

Solution Procedure for Zeroth-Order Equations

The solution for zeroth order equations involves the direct integration of the three coupled nonlinear partial differential equations. Typically, an iterative procedure is used to solve for the pressure distribution. The original analysis of Nelson and Nguyen (1988) proposed a method by which the coupled partial differential equations are reduced to coupled ordinary differential equations by approximating the circumferential gradients of the variables u_0 , v_0 and p_0 . At each axial step in the iterative procedure, the gradients with respect to β are computed based on the values of the variables at the previous step. An approximation scheme based on *Fast Fourier Transforms (FFT)* was used for this purpose. In the present analysis, a simpler method based on cubic splines is used. This method is more accurate as no truncation error is involved as in the FFT method. Also, convergence at higher eccentricities is achieved with relatively fewer iterations than the FFT method. It is also computationally more efficient as it does not involve the computation of CPU intensive trigonometric functions. A similar approach based on forward differences was reported by Simon and Frene (1992). Figure 4 illustrates typical subdivisions in the axial and circumferential directions. Note that the elliptical seal in Figure 5 represents a special case of the arbitrary profile shown in Figure 4.

The three steady state equations are arranged in the following fashion and integrated from inlet to the exit.

$$\begin{bmatrix} \frac{\partial p_0}{\partial z} \\ \frac{\partial u_0}{\partial z} \\ \frac{\partial v_0}{\partial z} \end{bmatrix} = \begin{bmatrix} g_u(u_0, v_0, p_0, \frac{\partial u_0}{\partial \beta}, \frac{\partial v_0}{\partial \beta}, \frac{\partial p_0}{\partial \beta}) \\ g_v(u_0, v_0, p_0, \frac{\partial u_0}{\partial \beta}, \frac{\partial v_0}{\partial \beta}, \frac{\partial p_0}{\partial \beta}) \\ g_p(u_0, v_0, p_0, \frac{\partial u_0}{\partial \beta}, \frac{\partial v_0}{\partial \beta}, \frac{\partial p_0}{\partial \beta}) \end{bmatrix} \quad (10)$$

The circumference is divided into segments of equal length. The above equations are integrated starting at each circumferential location in the direction of the corresponding point at the next axial step. When this step is reached, all the variables i.e., u_0 , v_0 and p_0 are known along the circumference. These values are then used to compute the circumferential gradients for the next step. In other words, at the i -th axial step, the circumferential

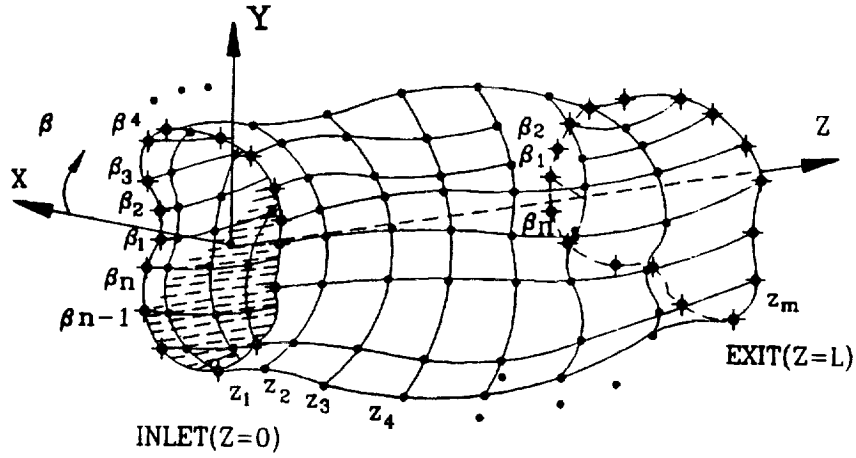


Figure 4: Circumferential and Axial Mesh Points for Numerical Integration

gradients are computed using the values of $u_{0(i-1,j)}$, $v_{0(i-1,j)}$ and $p_{0(i-1,j)}$ i.e., the values at the previous step. In the current analysis, an approximation scheme based on cubic splines is used to compute these gradients. Nelson and Nguyen used the simple Euler's method for the above numerical integration. For the current work, integration schemes based on 4th and 5th order Runge-Kutta method as well as predictor-corrector methods are used.

First Order Equations

The perturbed or first order equations are obtained for a small motion of the rotor about the steady state eccentric position using the following expressions. $h = h_0 + \epsilon h_1$, $p = p_0 + \epsilon p_1$, $u = u_0 + \epsilon u_1$ and $v = v_0 + \epsilon v_1$.

Substitution of these expressions into equations 1-3 and neglecting second and higher order terms yields the following first order equations.

$$h_0 \frac{\partial u_1}{\partial z} + \frac{h_0}{R} \frac{\partial v_1}{\partial \beta} + \frac{\partial h_1}{\partial z} u_1 + \frac{1}{R} \frac{\partial h_1}{\partial \beta} v_1 = -\frac{\partial h_1}{\partial t} - u_0 \frac{\partial h_1}{\partial z} - \frac{v_0}{R} \frac{\partial h_1}{\partial \beta} - \left(\frac{\partial u_0}{\partial z} + \frac{1}{R} \frac{\partial v_0}{\partial \beta} \right) h_1 \quad (11)$$

$$h_0 \frac{\partial u_1}{\partial t} + \frac{h_0}{\rho} \frac{\partial p_1}{\partial z} + h_0 u_0 \frac{\partial u_1}{\partial z} + \frac{h_0 v_0}{R} \frac{\partial u_1}{\partial \beta} + A_u u_1 + A_v v_1 = A_h h_1 \quad (12)$$

$$h_0 \frac{\partial v_1}{\partial t} + \frac{h_0}{\rho R} \frac{\partial p_1}{\partial \beta} + h_0 u_0 \frac{\partial v_1}{\partial z} + \frac{h_0 v_0}{R} \frac{\partial v_1}{\partial \beta} + B_u u_1 + B_v v_1 = B_h h_1 \quad (13)$$

where A_u , A_v , A_h , B_u , B_v and B_h are functions of steady state variables u_0 , v_0 , p_0 and their axial and circumferential gradients. These expressions are given in the appendix for both the Hir's and Moody's friction factors models.

The boundary conditions for the first order solution are (Nelson and Nguyen, 1988),

$$p_1(0, \beta) = -(1 + \xi)\rho u_0(0, \beta)u_1(0, \beta) \quad (14)$$

$$v_1(0, \beta) = 0 \quad (15)$$

$$p_1(L, \beta) = 0 \quad (16)$$

Assuming that the rotor whirls about its equilibrium position in an elliptical orbit whose semi-major and semi-minor axes are X_0 and Y_0 respectively, then the position of the center of the rotor relative to its static eccentric position is given by,

$$X = X_0 \cos \alpha \quad (17)$$

$$Y = Y_0 \sin \alpha \quad (18)$$

where $\alpha = \omega t$ and ω is the whirl frequency.

Let $\Delta x = \frac{X_0}{c_0}$, and $\Delta y = \frac{Y_0}{c_0}$ where c_0 is the nominal clearance, and;

$$\epsilon p_1 = \Delta \epsilon_x p_{1x} + \Delta \epsilon_y p_{1y} \quad (19)$$

$$\epsilon u_1 = \Delta \epsilon_x u_{1x} + \Delta \epsilon_y u_{1y} \quad (20)$$

$$\epsilon v_1 = \Delta \epsilon_x v_{1x} + \Delta \epsilon_y v_{1y} \quad (21)$$

$$\epsilon h_1 = \Delta \epsilon_x h_{1x} + \Delta \epsilon_y h_{1y} \quad (22)$$

$$h_{1x} = -c_0 \cos \alpha \cos \beta \quad (23)$$

$$h_{1y} = -c_0 \sin \alpha \sin \beta \quad (24)$$

Assume a solution of the form:

$$p_{1x} = a_1(z, \beta) \cos \alpha + a_2(z, \beta) \sin \alpha \quad (25)$$

$$u_{1x} = a_3(z, \beta) \cos \alpha + a_4(z, \beta) \sin \alpha \quad (26)$$

$$v_{1x} = a_5(z, \beta) \cos \alpha + a_6(z, \beta) \sin \alpha \quad (27)$$

$$p_{1y} = b_1(z, \beta) \cos \alpha + b_2(z, \beta) \sin \alpha \quad (28)$$

$$u_{1y} = b_3(z, \beta) \cos \alpha + b_4(z, \beta) \sin \alpha \quad (29)$$

$$v_{1y} = b_5(z, \beta) \cos \alpha + b_6(z, \beta) \sin \alpha \quad (30)$$

Using the above substitutions in the set of first order equations yields 12 coupled linear partial differential equations. The same solution procedure that is used for the zeroth order solution is used to numerically solve for variables a_i and b_i .

The first order boundary conditions are expressed in the assumed solution variables as:

$$a_1(0, \beta) = -(1 + \xi)\rho a_3(0, \beta) \quad (31)$$

$$a_2(0, \beta) = -(1 + \xi)\rho a_4(0, \beta) \quad (32)$$

$$a_5(0, \beta) = 0 \quad (33)$$

$$a_6(0, \beta) = 0 \quad (34)$$

$$a_1(L, \beta) = 0 \quad (35)$$

$$a_2(L, \beta) = 0 \quad (36)$$

Similar boundary conditions apply to governing equations involving b_i 's. The original analysis assumed these variables to be harmonic and separated them into two auxiliary functions of the form,

$$a_i = f_i(z)\cos\beta + g_i(z)\sin\beta \quad (37)$$

where f_i and g_i are assumed not to vary with β . Nelson and Nguyen 1988a) thereby apply a second separation of variables substitution to the first order differential equations (eqs. 14-16). While the above form of assumed solution yields results that agree with available experimental results, an examination of the numerical values of the functions $f_i(z)$ and $g_i(z)$ revealed a β dependence, particularly at eccentricities above (0.5). The inclusion of these circumferential gradients should therefore improve the solution at higher eccentricities.

The a_i and b_i in the current analysis are totally general functions of z and β which thereby avoids the mathematical contradiction discussed above. Furthermore, in many cases the results of the current approach show better agreement with experimental results than the earlier results.

The solution procedure for the 12 linear PDE's is exactly the same as that of the zeroth order solution. The solution is performed with 4-th and 5-th order Runge-Kutta method and also with a predictor-corrector method. Both methods almost identical results, the with Runge-Kutta based method being the fastest.

Dynamic Coefficients

The force components acting on the rotor due to its motion about a static eccentric position is given by integrating the first order pressure field, i.e.,

$$-\Delta F_x = \int_0^L \int_0^{2\pi} \epsilon p_1 \cos\beta R \, d\beta \, dz \quad (38)$$

$$-\Delta F_y = \int_0^L \int_0^{2\pi} \epsilon p_1 \sin\beta R \, d\beta \, dz \quad (39)$$

The following linearized force-motion model is used to define the rotordynamic coefficients. In this equation, X and Y define the relative displacement of the rotor and F_x , F_y are the components of the force due to first order pressure field.

$$\begin{aligned}
-\begin{Bmatrix} \Delta F_x \\ \Delta F_y \end{Bmatrix} &= \begin{bmatrix} K_{xx} & k_{xy} \\ -k_{yx} & K_{yy} \end{bmatrix} \begin{Bmatrix} x \\ y \end{Bmatrix} + \begin{bmatrix} C_{xx} & c_{xy} \\ -c_{yx} & C_{yy} \end{bmatrix} \begin{Bmatrix} \dot{x} \\ \dot{y} \end{Bmatrix} \\
&+ \begin{bmatrix} M_{xx} & m_{xy} \\ -m_{yx} & m_{yy} \end{bmatrix} \begin{Bmatrix} \ddot{x} \\ \ddot{y} \end{Bmatrix} \quad (40)
\end{aligned}$$

The original analysis discretized the circumference into a number of strips and the function values (f_i, g_i) are assumed to be independent of β over each strip. The current method improves this approach by allowing the a_i and b_i to vary over each strip in obtaining the rotordynamic coefficients.

Substitute eqs. 28-33 into 22-27 and in turn substitute the results into eqs. 43-45. Also substitute eqs. 20 and 21 into 43-45. This yields:

$$K_{xx} - M_{xx}\omega^2 = \frac{1}{c_0} \int_0^L \int_0^{2\pi} a_1 \cos\beta R \, d\beta \, dz \quad (41)$$

$$c_{xy}\omega = \frac{1}{c_0} \int_0^L \int_0^{2\pi} b_1 \cos\beta R \, d\beta \, dz \quad (42)$$

$$-k_{yx} + m_{yx}\omega^2 = \frac{1}{c_0} \int_0^L \int_0^{2\pi} a_1 \sin\beta R \, d\beta \, dz \quad (43)$$

$$C_{yy}\omega = \frac{1}{c_0} \int_0^L \int_0^{2\pi} b_1 \sin\beta R \, d\beta \, dz \quad (44)$$

$$-C_{xx}\omega = \frac{1}{c_0} \int_0^L \int_0^{2\pi} a_2 \cos\beta R \, d\beta \, dz \quad (45)$$

$$k_{yx} - m_{xy}\omega^2 = \frac{1}{c_0} \int_0^L \int_0^{2\pi} b_2 \cos\beta R \, d\beta \, dz \quad (46)$$

$$c_{yx}\omega = \frac{1}{c_0} \int_0^L \int_0^{2\pi} a_2 \sin\beta R \, d\beta \, dz \quad (47)$$

$$K_{yy} - m_{yy}\omega^2 = \frac{1}{c_0} \int_0^L \int_0^{2\pi} b_2 \sin\beta R \, d\beta \, dz \quad (48)$$

These 8 equations are evaluated for at least two whirl frequencies to obtain solutions for the 12 dynamic coefficients. A least squares approach is employed for this step. The 2D integration performed numerically are an improvement over the average value approach employed by the previous researchers.

Dynamic Coefficients based on External Load Specification

In some cases, it is possible to specify the angle at which external load is supported by the seal during the operation of the turbomachine. This external load is equal and opposite to the resultant seal force. A new method of computing the rotordynamic coefficients based on this load angle is described below.

The static operating position of the rotor is located iteratively such that there is equilibrium between the external specified load and the resultant seal force. The angle at which

the resultant seal force acts is forced to align (180°) with the specified external load angle. For example, unit 3-01, an experimental seal under design at NASA (results to be discussed later) supports the external load at a constant angle of 290° in the rotor coordinate system.

Determination of Steady State Force Equilibrium Position

A modified Newton-Raphson approach is used in two dimensions to locate the operating position. At the steady state equilibrium position,

$$f_x = F_x - W \sin \beta = 0$$

$$f_y = F_y - W \cos \beta = 0$$

The modified 2-D Newton-Raphson iteration procedure is described below.

$$\Delta x \frac{\partial f_x}{\partial x} |_{x_i, y_i} + \Delta y \frac{\partial f_x}{\partial y} |_{x_i, y_i} + f_x |_{x_i, y_i} = 0 \quad (49)$$

$$\Delta x \frac{\partial f_y}{\partial x} |_{x_i, y_i} + \Delta y \frac{\partial f_y}{\partial y} |_{x_i, y_i} + f_y |_{x_i, y_i} = 0 \quad (50)$$

The seal forces F_x and F_y are computed using an initial guess of rotor position (x_i, y_i) . The gradients $\frac{\partial f_x}{\partial x}$, $\frac{\partial f_x}{\partial y}$, $\frac{\partial f_y}{\partial x}$ and $\frac{\partial f_y}{\partial y}$ are computed using finite differences about (x_i, y_i) . This iterative procedure is repeated until the specified external load is balanced by the resultant seal forces. Once this equilibrium position is attained, the remaining analysis proceeds as before.

Verification Case: Allaire, et. al.

The first illustrative example compares the original and current Nguyen-Nelson approach results to the "short seal" solution employed by Allaire. All three approaches show similar direct stiffness, damping and cross-coupled stiffness vs. eccentricity as seen in figures 6, 7 and 8 respectively.

<i>Seal Parameters for Allaire et al. case</i>	
seal length	40.6 mm (1.60 in)
rotor radius	39.9 mm (1.57 in)
c_i	0.14 mm (0.0055 in)
c_e	0.14 mm (0.0055 in)
c_o	0.14 mm (0.0055 in)
fluid	LO2
density, ρ	57.657 kg/m ³ (3.60 lbm/ft ³)
viscosity, μ	7.4396×10^{-6} Pa-s (1.5538×10^{-7} lb-s/ft ²)
ΔP	7.26 MPa (1050 psi)
rotor speed	23700 rpm
friction factor	Moody's
relative	0.0 (rotor)
roughness, $e/2c_o$	0.000001 (stator)
pre-swirl ratio	0.1
inlet loss, ξ	0.5

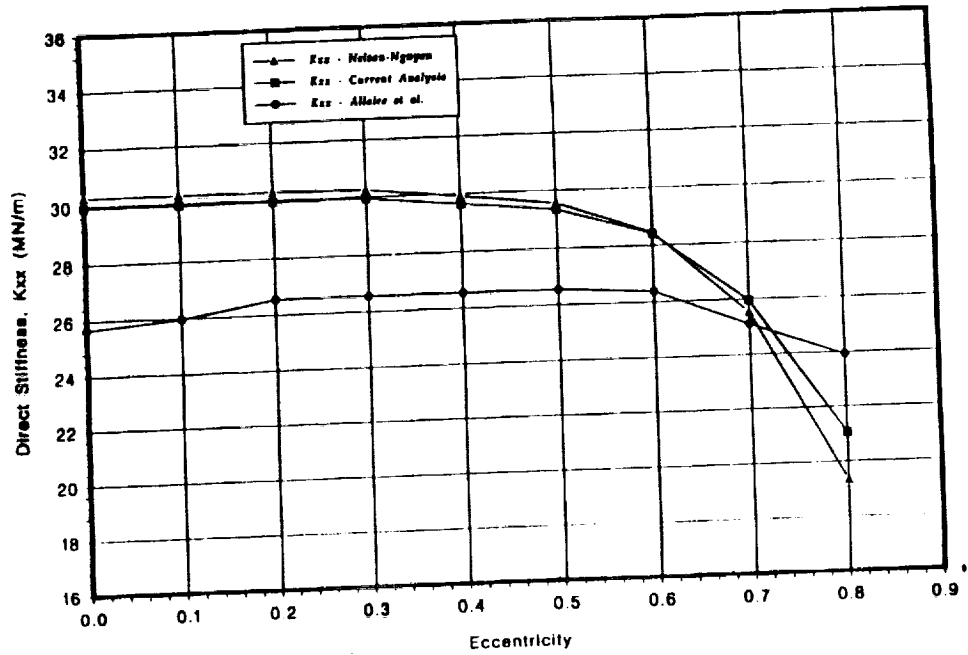


Figure 5: Direct Stiffness .vs. Eccentricity for Allaire Example

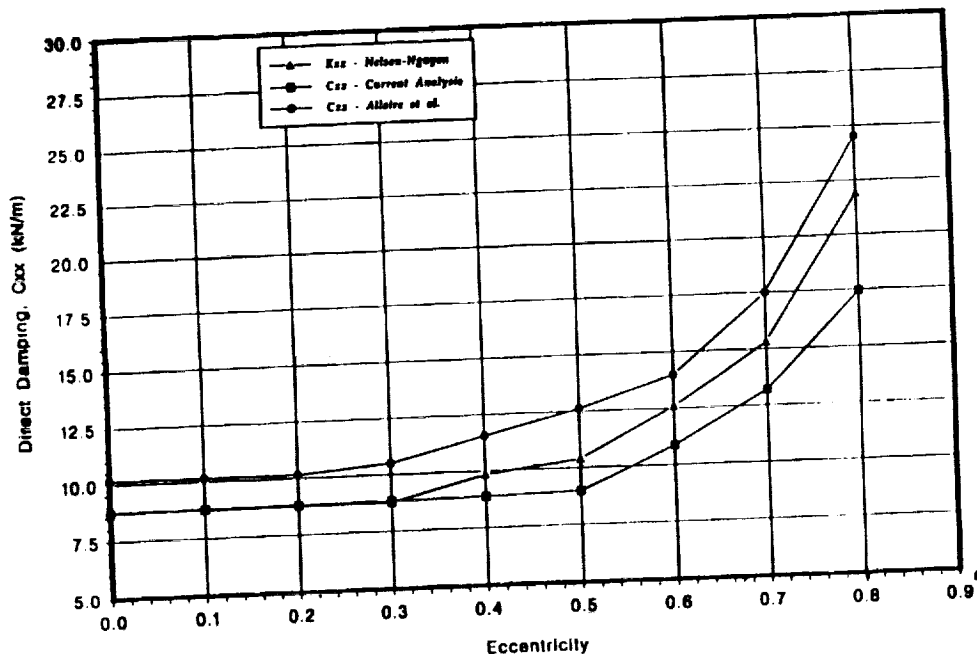


Figure 6: Direct Damping .vs. Eccentricity for Allaire Example

EXAMPLE OF AN ARBITRARY PROFILE SEAL: AN ELLIPTICAL SEAL

The above analysis for an arbitrary profile is applied to the case of an elliptical seal with axially varying curvature. The results for a similar linearly tapered elliptical seal, were initially reported by San Andres (1992). The motivation for this study is two fold. The first is to show the general steps involved in the analysis of arbitrary profile seals and the other is to show, in qualitative terms, the effect of a change in profile on the dynamic coefficients.

Two cases of curvature are considered for this analysis: one with a linear axial profile and the other a quadratic axial profile. For this study, the mid-point clearance of the quadratic profile is made 75% of $(c_i + c_e)/2$, i.e., 0.75 times the mid-point clearance of a linear profile with similar inlet and exit clearances.

The equation of an ellipse is given by,

$$x = a \cos \beta \quad (51)$$

$$y = b \sin \beta \quad (52)$$

where a and b are the semi-major and semi-minor axes respectively. At any angular position β along the circumference, the radius r of the ellipse is given by,

$$r = \sqrt{(a \cos \beta)^2 + (b \sin \beta)^2} \quad (53)$$

and the clearance c at this location is given by,

$$c = r - R \quad (54)$$

where R is the radius of the rotor.

If the semi-major and semi-minor axes of the ellipse vary in some functional form along the length of the seal, the clearance is given by,

$$c(z, \beta) = \sqrt{(f_1(z) \cos \beta)^2 + (f_2(z) \sin \beta)^2} - R \quad (55)$$

where $f_1(z)$ and $f_2(z)$ are the semi-major and semi-minor axes variations along the z -axis. The gradients of this clearance function are given in the appendix.

The ellipticity δ is defined as (Fig. 5),

$$\delta = \frac{c_x - c_y}{c_x} \quad (56)$$

where c_x and c_y are clearances at semi-major and semi-minor axes respectively and,

$$c_x = c_i \text{ at inlet}$$

$$c_x = c_e \text{ at exit}$$

and from above,

$$c_y = c_x(1 - \delta) \quad (57)$$

When $\delta = 0$, the ellipse reduces to a circle and for $\delta = 1$, the seal contacts the rotor. The appendix provides the functions $f_1(z)$ and $f_2(z)$ for a linear profile and a quadratic profile, as a function of delta. The results shown are for a centered seal as a function of ellipticity. The dynamic coefficients are normalized with respect to the coefficients for the linear profile case at $\delta = 0$. The values used for this normalization are $K_{xx} = 44975 \text{ kN/m}$ (256883 lb/in), $C_{xx} = 21.78 \text{ kN-s/m}$ (124.4 lb-s/in) and $k_{xy} = 15821 \text{ kN/m}$ (90364 lb/in). The seal parameters for this case are given below.

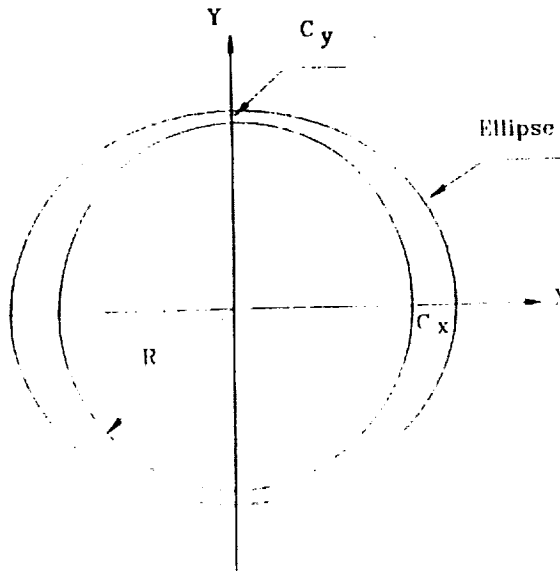


Figure 7: Diagram for Deriving Elliptical Seal Clearance Expression

<i>Seal Parameters for Elliptical Seal</i>	
seal length	16.66 mm (0.656 in)
rotor radius	48.39 mm (1.905 in)
c_i	0.069 mm (0.00273 in)
c_e	0.099 mm (0.00390 in)
c_0	0.069 mm (0.00273 in)
fluid	LO2
density, ρ	1041.7 kg/m ³ (65.03 lbm/ft ³)
viscosity μ	129.6 $\times 10^{-6}$ Pa-s (0.188 $\times 10^{-8}$ lb-s/ft ²)
ΔP	25.39 MPa (3681 psi)
rotor speed	22700 rpm
friction factor	Moody's
relative	0.0 (rotor)
roughness, $e/2c_0$	0.03 (stator)
pre-swirl ratio	0.2
inlet loss, ξ	0.33

The plot for direct stiffness (Fig. 9) shows the effect of a small change in profile on the direct stiffness. For the linear case, there is a complete loss of stiffness at around $\delta = 0.65$. The stiffness for the quadratic profile is almost twice that of the linear profile. Also, it retains its stiffness over a much wider range than the linear profile. The difference in the other coefficients (Figs. 10,11) are relatively small.

CASE STUDY OF A DISTORTED SEAL

The distorted clearance profile for an interstage seal of the Space Shuttle Main Engine High Pressure Oxygen Turbopump (SSME-ATD-HPOTP) is shown in Fig. 1. The distorted

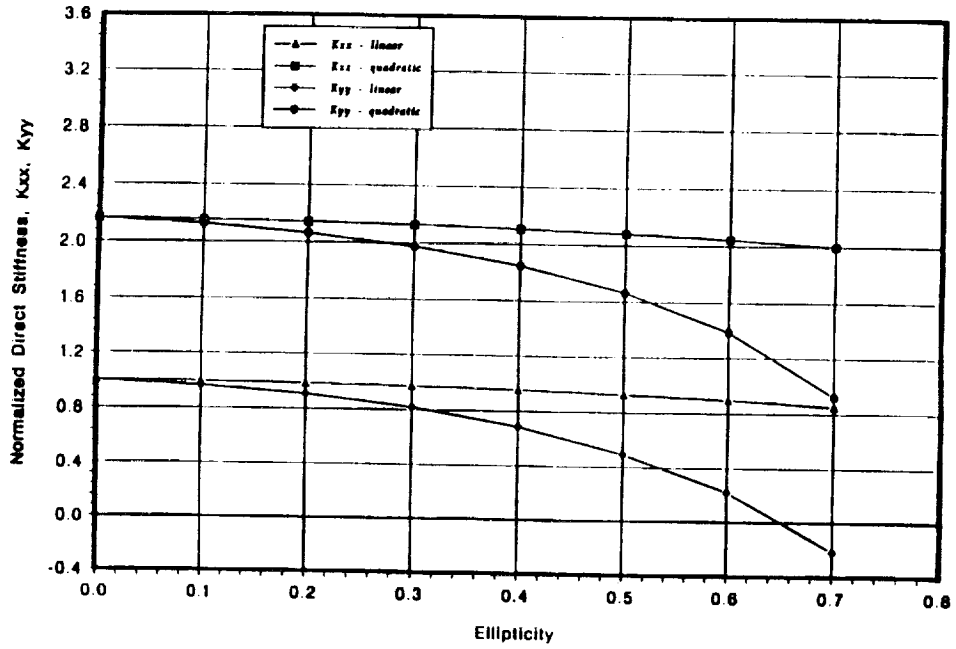


Figure 8: Normalized Direct Stiffness .vs. Ellipticity (Elliptical Seal)

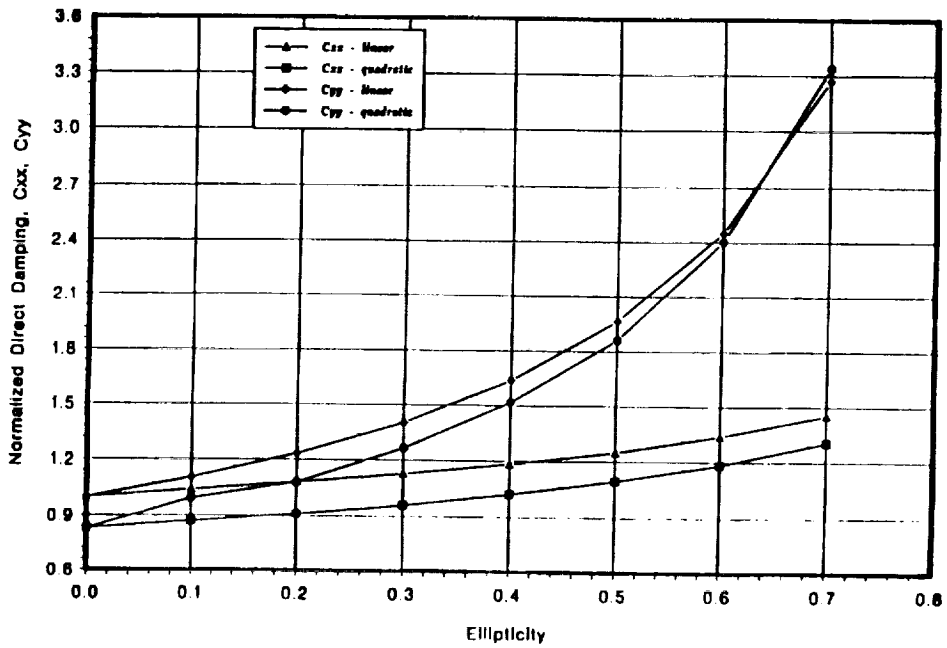


Figure 9: Normalized Direct Damping .vs. Ellipticity (Elliptical Seal)

clearance profile of this seal is obtained from a thermoelastic analysis. The clearances are provided at six axial planes along the length of the seal with 68 clearances at each plane. The clearances along the circumference are located roughly equidistant.

The rotordynamic coefficients of the distorted profile are compared with those computed using average clearances at inlet and outlet respectively. The geometry and operating conditions at full power level FPL are given in the following table.

seal length	16.66 mm (0.656 in)
rotor radius	48.39 mm (1.905 in)
avg. c_i	0.149 mm (5.87 mils)
avg. c_e	0.148 mm (5.81 mils)
c_0	0.149 mm (5.87 mils)
fluid	LO2
density, ρ	1041.7 kg/m ³ (65.03 lbm/ft ³)
viscosity μ	129.6 $\times 10^{-6}$ Pa-s (0.188 $\times 10^{-8}$ lb-s/ft ²)
ΔP	35.25 MPa (5112 psi)
rotor speed	25000 rpm
friction factor	Moody's
relative	0.0 (rotor)
roughness, $e/2c_0$	0.8518 (stator)
pre-swirl ratio	0.2
inlet loss	0.3

The distorted seal profile is fitted with bi-cubic splines. The purpose of this spline fitting is two fold; one is to interpolate clearances at any given axial and circumferential location and the other is to numerically compute axial and circumferential gradients of the seal profile at any required location.

According to the manufacturer's specifications, the side-load on the seal acts at a constant angle of 290°. The seal coefficients for this variable profile seal are computed as a function of side-load acting at this angle.

Figure 12. shows the relation between seal forces and eccentricity. No load operation requires the seal to be slightly off-centered due to the distortion in the seal. Figs. 13,14 and 15 show how the dynamic coefficients vary with externally applied load and the effects of distorted clearance profile versus average profile (average of clearances at the inlet and exit circumferences). The coefficients are seen to be sensitive to high loads and also show significant changes due to the distorted profile, i.e., see Fig 15.

CONCLUSIONS

The current approach has improved on the original Nelson-Nguyen method (NNM) by;

- (a) Employing a continuous interpolation of the first order variables in the circumferential direction, and
- (b) Utilizing cubic splines instead of Fourier series for the circumferential interpolation of both zeroth and first order variables.

In addition the current method models seals with arbitrary clearance profiles in the circumferential and axial directions. This capability was demonstrated with the operating seal

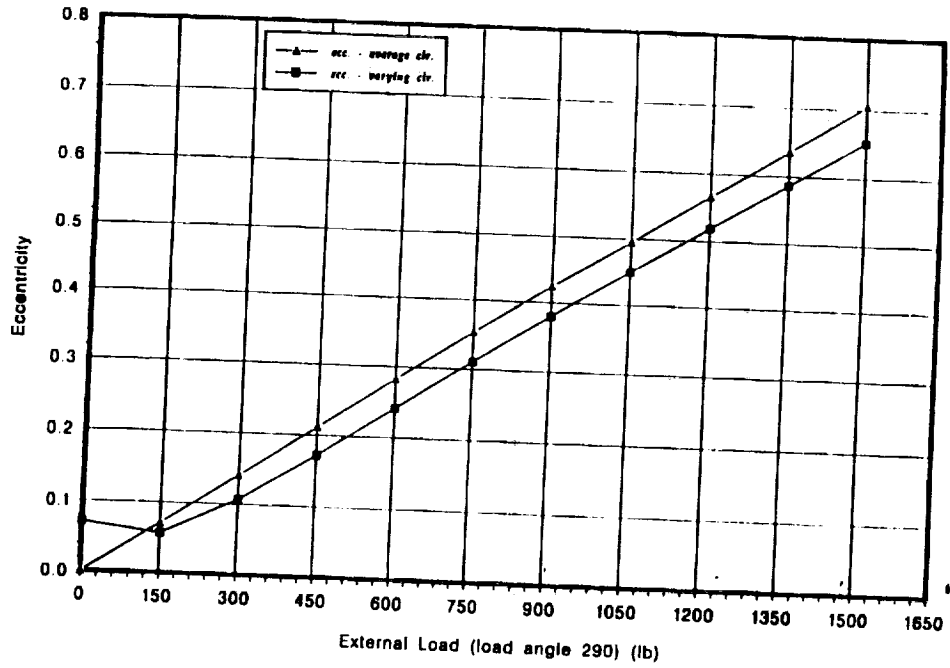


Figure 10: Eccentricity .vs. Preload for Operating Seal Clearance Profile (Fig 1.)

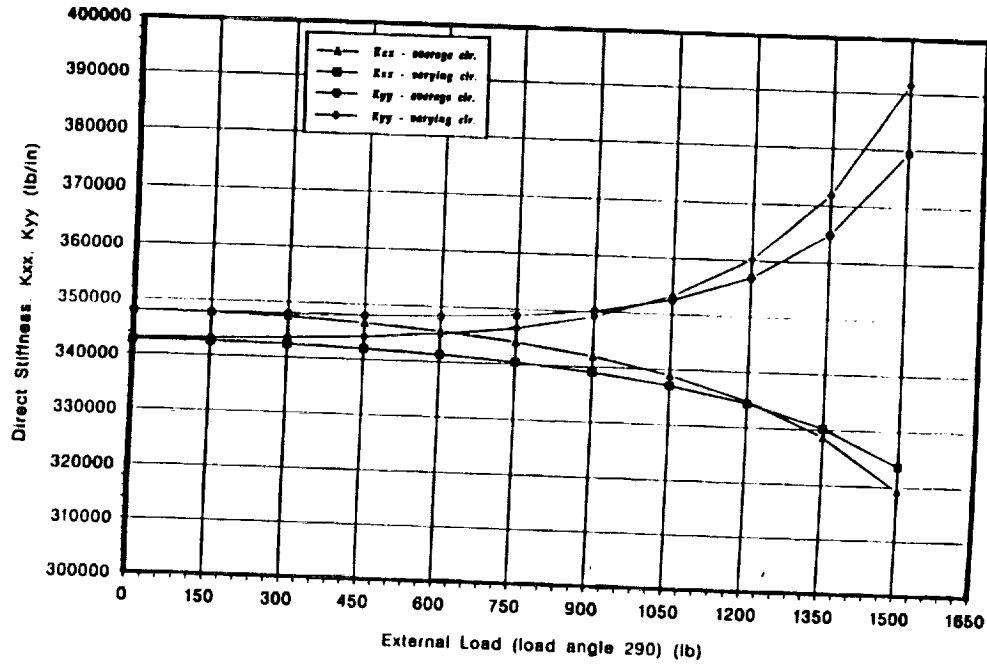


Figure 11: Direct Stiffness .vs. Preload for Operating Seal Clearance Profile (Fig. 1)

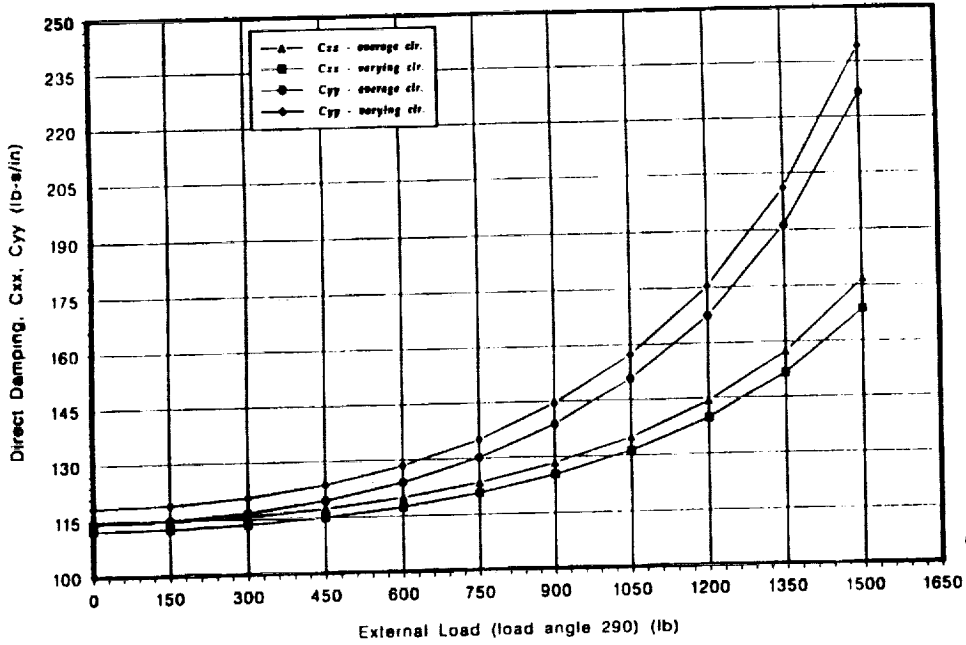


Figure 12: Direct Damping vs. Preload for Operating Seal Clearance Profile (Fig. 1)

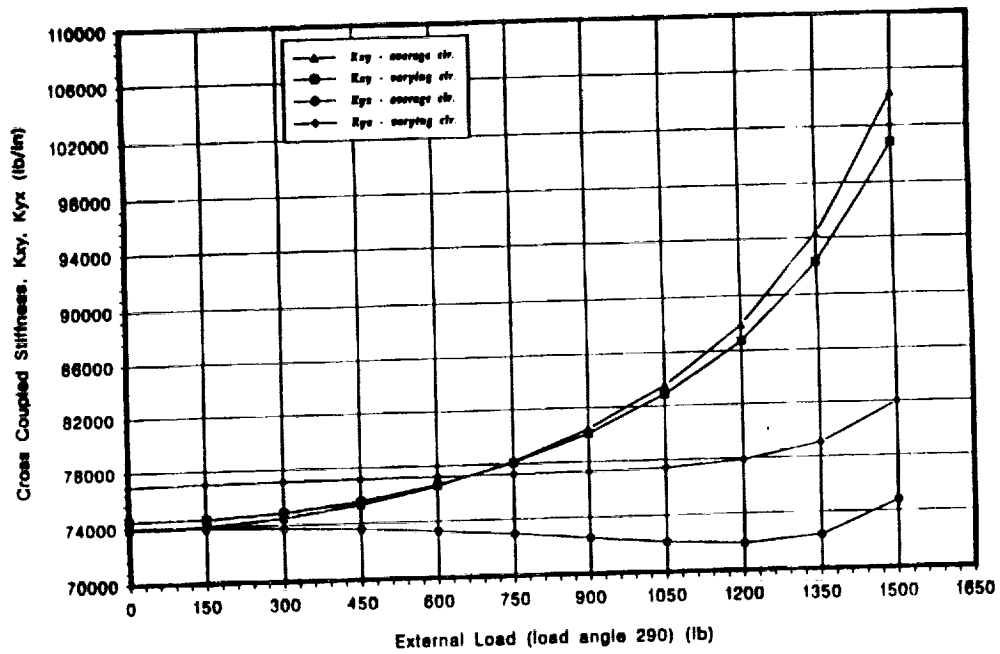


Figure 13: Cross Coupled Stiffness vs. Preload for Operating Seal Clearance Profile (Fig. 1)

profile of a SSME-HPOTP seal. Finally a procedure is presented for locating the operating equilibrium position of the seal given the preload acting on the seal.

ACKNOWLEDGMENTS

The authors wish to thank NASA Marshall for supporting this research and to acknowledge the technical support provided by Mark Darden, Chip Franks, Kerry Funston, Eric Earhart and Barry Whitsett.

REFERENCES

- Allaire, P.E., et al., 1978, "Dynamics of Short Eccentric Plain Seals With High Axial Reynolds Numbers," *J. Spacecraft, AIAA*, Vol.15, No.6, Nov.-Dec.
- Black, H.F., Allaire, 1969, "Effects of Hydraulic Forces in Annular Pressure Seals on the Vibrations of Centrifugal Pump Rotors," *Journal of Mechanical Engineering Science*, Vol. 11, pp. 206-213.
- Black, H.F., Allaire, P.E., and L.E. Barrett, 1981, "Inlet Flow Swirl in Short Turbulent Annular Seals," 9-th International Conference on Fluid Sealing, BHRA Fluid Engineering, Leeuwenhorst, The Netherlands, April.
- Childs, D.W., 1983a, "Dynamic Analysis of Turbulent Annular Seals Based on Hirs Lubrication Equation," *ASME Journal of Lubrication Technology*, Vol. 105, pp 429-436.
- Childs, D.W., 1983b, "Finite Length Solutions for Rotordynamic Coefficients of Turbulent Annular Seals," *ASME Journal of Lubrication Technology*, Vol. 105, pp. 437-444.
- Nguyen, D.T., 1988, "Analysis of Eccentric Annular Pressure Seals: A New Solution Procedure for Determining Reactive Force and Rotordynamic Coefficients", Ph.D. Dissertation, Texas A&M University, College Station, TX.
- Nelson, C., Nguyen, D.T., 1988a, "Analysis of Eccentric Annular Seals: Part I - A New Solution Using Fast Fourier Transforms for Determining Hydrodynamic Force," *ASME Journal of Tribology*, Vol 110, pp. 335-360.
- Nelson, C., and Nguyen, D.T., 1988b, "Analysis of Eccentric Annular Seals: Part II - Effects of Eccentricity on Rotordynamic Coefficients," *ASME Journal of Tribology*, Vol. 110, pp. 361-366.
- San Andres, L., 1991, "Analysis of Variable Properties Turbulent Annular Seals," *ASME Jour. of Tribology*, Vol. 113, pp. 694-702.
- San Andres, 1992, Personal Communications.
- Scharrer, J.K., and D.J. Nunez, 1989, "The SSME HPFTP Wavy Interstage Seal: I - Seal Analysis," *Proceedings of the 1989 ASME Vibrations Conference, Machinery Dynamics - Applications and Vibration Control Problems, DE-Vol. 18-2*.
- Simon, F., and Frene J., 1992, "Analysis of Incompressible Flow in Annular Pressure Seals", *STLE/ASME Tribology Conference, St. Louis, MO, 1991*.

APPENDIX

The coefficient expressions for the first order equations are defined as

$$A_u = h_0 \frac{\partial u_0}{\partial z} + \left(\frac{F_{s0}}{U_{s0}} + \frac{F_{r0}}{U_{r0}} \right) + (f_s U_{s0} + f_r U_{r0}) \quad (58)$$

$$A_v = \frac{h_0}{R} \frac{\partial u_0}{\partial \beta} + u_0 v_0 \frac{F_{s0}}{U_{s0}} + u_0 (v_0 - w) \frac{F_{r0}}{U_{r0}} \quad (59)$$

$$A_h = -\frac{1}{\rho} \frac{\partial p_0}{\partial z} - u_0 \frac{\partial u_0}{\partial z} - \frac{v_0}{R} \frac{\partial v_0}{\partial \beta} + \frac{u_0}{h_0} (h_{s0} U_{s0} + h_r U_{r0}) \quad (60)$$

$$B_u = h_0 \frac{\partial v_0}{\partial z} + u_0 v_0 \frac{F_{s0}}{U_{s0}} + u_0 (v_0 - w) \frac{F_{r0}}{U_{r0}} \quad (61)$$

$$B_v = \frac{h_0}{R} \frac{\partial v_0}{\partial \beta} + v_0^2 \frac{F_{s0}}{U_{s0}} + (v_0 - w)^2 \frac{F_{r0}}{U_{r0}} + f_s U_{s0} + f_r U_{r0} \quad (62)$$

$$B_h = -\frac{1}{\rho} \frac{\partial p_0}{\partial \beta} - u_0 \frac{\partial v_0}{\partial z} - \frac{v_0}{R} \frac{\partial v_0}{\partial \beta} + v_0 U_{s0} \frac{h_{s0}}{h_0} + (v_0 - w) U_{r0} \frac{h_r}{h_0} \quad (63)$$

$$(64)$$

with further definitions for Moody's and Hirs' friction models given in the following table:

Moody's Model	Hirs' Model
$U_{r0} = (u_0^2 + (v_0 - w)^2)^{1/2}$	$U_{r0} = (u_0^2 + (v_0 - w)^2)^{1/2}$
$U_{s0} = (u_0^2 + v_0^2)^{1/2}$	$U_{s0} = (u_0^2 + v_0^2)^{1/2}$
$R_{r0} = \frac{2\rho h_0}{\mu} (u_0^2 + (v_0 - w)^2)^{1/2}$	$R_{r0} = \frac{2\rho h_0}{\mu} (u_0^2 + (v_0 - w)^2)^{1/2}$
$R_{s0} = \frac{2\rho h_0}{\mu} (u_0^2 + v_0^2)^{1/2}$	$R_{s0} = \frac{2\rho h_0}{\mu} (u_0^2 + v_0^2)^{1/2}$
$f_{r0} = \frac{0.0055}{4} [1 + (10^4 \frac{K_r}{h_0} + 10^6 \frac{1}{R_{r0}})^{1/3}]$	$f_{r0} = n_r [\frac{2\rho h_0}{\mu} R_{r0}]^{m_r}$
$f_{s0} = \frac{0.0055}{4} [1 + (10^4 \frac{K_s}{h_0} + 10^6 \frac{1}{R_{s0}})^{1/3}]$	$f_{s0} = n_s [\frac{2\rho h_0}{\mu} R_{s0}]^{m_s}$
$g_{r0} = \frac{0.0055 \times 10^6}{12 R_{r0}} (10^4 \frac{K_r}{h_0} + \frac{10^6}{R_{r0}})^{-2/3}$	$g_{r0} = -m_r n_r [R_{r0}]^{m_r}$
$g_{s0} = \frac{0.0055 \times 10^6}{12 R_{s0}} (10^4 \frac{K_s}{h_0} + \frac{10^6}{R_{s0}})^{-2/3}$	$g_{s0} = -m_s n_s [R_{s0}]^{m_s}$
$h_{r0} = \frac{0.0055}{12} (10^4 \frac{K_r}{h_0} + \frac{10^6}{R_{r0}})^{1/3}$	$h_{r0} = -m_r n_r [R_{r0}]^{m_r}$
$h_{s0} = \frac{0.0055}{12} (10^4 \frac{K_s}{h_0} + \frac{10^6}{R_{s0}})^{1/3}$	$h_{s0} = -m_s n_s [R_{s0}]^{m_s}$
$\bar{f}_r = f_{r0}$	$\bar{f}_r = f_{r0}$
$\bar{f}_s = f_{s0}$	$\bar{f}_s = f_{s0}$
$f_r = f_{r0}/2$	$f_r = f_{r0}/2$
$f_s = f_{s0}/2$	$f_s = f_{s0}/2$
$g_r = g_{r0}/2$	$g_r = g_{r0}/2$
$g_s = g_{s0}/2$	$g_s = g_{s0}/2$
$h_r = h_{r0}/2$	$h_r = g_{r0}/2$
$h_s = h_{s0}/2$	$h_s = g_{s0}/2$
$F_{r0} = \frac{f_r - g_r}{2}$	$F_{r0} = \frac{f_r - g_r}{2}$
$F_{s0} = \frac{f_s - g_s}{2}$	$F_{s0} = \frac{f_s - g_s}{2}$

The first-order governing equations are expressed in terms of the a_i and b_i functions as;

$$\begin{aligned} \frac{h_0}{\rho} \frac{\partial a_1}{\partial z} + (A_u - u_0 \frac{\partial h_0}{\partial z}) a_3 + h_0 \omega a_4 (A_v - \frac{u_0}{R} \frac{\partial h_0}{\partial \beta}) a_5 = -\frac{h_0 v_0}{R} \frac{\partial a_3}{\partial \beta} + \frac{h_0 u_0}{R} \frac{\partial a_5}{\partial \beta} \\ - c_0 [(A_h + u_0 (\frac{\partial u_0}{\partial z} + \frac{1}{R} \frac{\partial v_0}{\partial \beta})) \cos \beta - \frac{u_0 v_0}{R} \sin \beta] \end{aligned} \quad (65)$$

$$\begin{aligned} \frac{h_0}{\rho} \frac{\partial a_2}{\partial z} - h_0 \omega a_3 + (A_u - u_0 \frac{\partial h_0}{\partial z}) a_4 + (A_v - \frac{u_0}{R} \frac{\partial h_0}{\partial \beta}) a_6 = c_0 \omega u_0 \cos \beta - \frac{h_0 v_0}{R} \frac{\partial a_4}{\partial \beta} \\ + \frac{h_0 u_0}{R} \frac{\partial a_6}{\partial \beta} \end{aligned} \quad (66)$$

$$h_0 \frac{\partial a_3}{\partial z} + \frac{\partial h_0}{\partial z} a_3 + \frac{1}{R} \frac{\partial h_0}{\partial \beta} a_5 = c_0 [(\frac{\partial u_0}{\partial z} + \frac{1}{R} \frac{\partial v_0}{\partial \beta}) \cos \beta - \frac{v_0}{R} \sin \beta] - \frac{h_0}{R} \frac{\partial a_5}{\partial \beta} \quad (67)$$

$$h_0 \frac{\partial a_4}{\partial z} + \frac{\partial h_0}{\partial z} a_4 + \frac{1}{R} \frac{\partial h_0}{\partial \beta} a_6 = -c_0 \omega \cos \beta - \frac{h_0}{R} \frac{\partial a_6}{\partial \beta} \quad (68)$$

$$h_0 u_0 \frac{\partial a_5}{\partial z} + B_u a_3 + B_v a_5 + h_0 \omega a_6 = -c_0 B_h \cos \beta - \frac{h_0}{R \rho} \frac{\partial a_1}{\partial \beta} - \frac{h_0 v_0}{R} \frac{\partial a_5}{\partial \beta} \quad (69)$$

$$h_0 u_0 \frac{\partial a_6}{\partial z} + B_u a_4 - h_0 \omega a_5 + B_v a_6 = -\frac{h_0}{R \rho} \frac{\partial a_2}{\partial \beta} - \frac{h_0 v_0}{R} \frac{\partial a_6}{\partial \beta} \quad (70)$$

$$\begin{aligned} \frac{h_0}{\rho} \frac{\partial b_1}{\partial z} + (A_u - u_0 \frac{\partial h_0}{\partial z}) b_3 + h_0 \omega b_4 + (A_v - \frac{u_0}{R} \frac{\partial h_0}{\partial \beta}) b_5 = -c_0 \omega u_0 \sin \beta - \frac{h_0 v_0}{R} \frac{\partial b_3}{\partial \beta} \\ + \frac{h_0 u_0}{R} \frac{\partial b_5}{\partial \beta} \end{aligned} \quad (71)$$

$$\begin{aligned} \frac{h_0}{\rho} \frac{\partial b_2}{\partial z} - h_0 \omega b_3 + (A_u - u_0 \frac{\partial h_0}{\partial z}) b_4 + (A_v - \frac{u_0}{R} \frac{\partial h_0}{\partial \beta}) b_6 \\ = -c_0 [(A_h + u_0 (\frac{\partial u_0}{\partial z} + \frac{1}{R} \frac{\partial v_0}{\partial \beta})) \sin \beta + \frac{u_0 v_0}{R} \cos \beta] - \frac{h_0 v_0}{R} \frac{\partial b_4}{\partial \beta} + \frac{h_0 u_0}{R} \frac{\partial b_6}{\partial \beta} \end{aligned} \quad (72)$$

$$h_0 \frac{\partial b_3}{\partial z} + \frac{\partial h_0}{\partial z} b_3 + \frac{1}{R} \frac{\partial h_0}{\partial \beta} b_5 = c_0 \omega \sin \beta - \frac{h_0}{R} \frac{\partial b_5}{\partial \beta} \quad (73)$$

$$h_0 \frac{\partial b_4}{\partial z} + \frac{\partial h_0}{\partial z} b_4 + \frac{1}{R} \frac{\partial h_0}{\partial \beta} b_6 = c_0 [\frac{v_0}{R} \cos \beta + (\frac{\partial u_0}{\partial z} + \frac{1}{R} \frac{\partial v_0}{\partial \beta}) \sin \beta] - \frac{h_0}{R} \frac{\partial b_6}{\partial \beta} \quad (74)$$

$$h_0 u_0 \frac{\partial b_5}{\partial z} + B_u b_3 + B_v b_5 + h_0 \omega b_6 = -\frac{h_0}{R \rho} \frac{\partial b_1}{\partial \beta} - \frac{h_0 v_0}{R} \frac{\partial b_5}{\partial \beta} \quad (75)$$

$$h_0 u_0 \frac{\partial b_6}{\partial z} + B_u b_4 - h_0 \omega b_5 + B_v b_6 = -c_0 B_h \sin \beta - \frac{h_0}{R \rho} \frac{\partial b_2}{\partial \beta} - \frac{h_0 v_0}{R} \frac{\partial b_6}{\partial \beta} \quad (76)$$

The clearance functions for the elliptical seal are given in the next table as:

<i>linear taper</i>	<i>quadratic curve</i>
$f_1(z) = a_1 + a_2z$	$f_1(z) = a_1 + a_2z + a_3z^2$
$f_2(z) = b_1 + b_2z$	$f_2(z) = b_1 + b_2z + b_3z^2$
$\frac{\partial f_1}{\partial z} = a_2$	$\frac{\partial f_1}{\partial z} = a_2 + 2a_3z$
$\frac{\partial f_2}{\partial z} = b_2$	$\frac{\partial f_2}{\partial z} = b_2 + 2b_3z$
$a_1 = R + c_i$	$a_1 = R + c_i$
$a_2 = \frac{1}{L}(c_e - c_i)$	$a_2 = \frac{-1}{L}(c_e - 4c_m + 3c_i)$
	$a_3 = \frac{2}{L^2}(c_e - 2c_m + c_i)$
$b_1 = R + (1 - \delta)c_i$	$b_1 = R + (1 - \delta)c_i$
$b_2 = \frac{1}{L}(1 - \delta)(c_e - c_i)$	$b_2 = \frac{-1}{L}(1 - \delta)(c_e - 4c_m + 3c_i)$
	$b_3 = \frac{2}{L}(1 - \delta)(c_e - 2c_m + c_i)$

Gradients of the clearance function for elliptical seal are given by;

$$c(z, \beta) = \sqrt{(f_1(z)\cos\beta)^2 + (f_2(z)\sin\beta)^2} - R \quad (77)$$

$$\frac{\partial c}{\partial z} = \frac{f_1 f_1' \cos^2 \beta + f_2 f_2' \sin^2 \beta}{\sqrt{(f_1 \cos \beta)^2 + (f_2 \sin \beta)^2}} \quad (78)$$

$$\frac{\partial c}{\partial \beta} = \frac{(f_2^2 - f_1^2) \cos \beta \sin \beta}{\sqrt{(f_1 \cos \beta)^2 + (f_2 \sin \beta)^2}} \quad (79)$$

